isvr Institute of Sound and Vibration Research

Ground Vibration Generated by a Harmonic Load Moving in a Circular Tunnel in a Layered Ground

X. Sheng, C.J.C. Jones and D.J. Thompson

ISVR Technical Memorandum No 890

July 2002

University of Southampton

SCIENTIFIC PUBLICATIONS BY THE ISVR

Technical Reports are published to promote timely dissemination of research results by ISVR personnel. This medium permits more detailed presentation than is usually acceptable for scientific journals. Responsibility for both the content and any opinions expressed rests entirely with the author(s).

Technical Memoranda are produced to enable the early or preliminary release of information by ISVR personnel where such release is deemed to the appropriate. Information contained in these memoranda may be incomplete, or form part of a continuing programme; this should be borne in mind when using or quoting from these documents.

Contract Reports are produced to record the results of scientific work carried out for sponsors, under contract. The ISVR treats these reports as confidential to sponsors and does not make them available for general circulation. Individual sponsors may, however, authorize subsequent release of the material.

UNIVERSITY OF SOUTHAMPTON

INSTITUTE OF SOUND AND VIBRATION RESEARCH

DYNAMICS GROUP

Ground Vibration Generated by a Harmonic Load Moving in a Circular Tunnel in a Layered Ground

by

X. Sheng, C.J.C. Jones and D.J. Thompson

ISVR Technical Memorandum No: 890

July 2002

Authorised for issue by
Dr M.J. Brennan
Group Chairman

GROUND VIBRATION GENERATED BY A HARMONIC LOAD MOVING IN A CIRCULAR TUNNEL IN A LAYERED GROUND

X Sheng, C J C Jones and D J Thompson

ABSTRACT

In this paper, a predictive model has been developed for ground vibration generated by a stationary or moving harmonic load applied in a circular lined or unlined tunnel in a layered ground. This study is the first step to use *discrete wavenumber methods* to model ground vibration from underground trains. Discrete wavenumber methods can be *the discrete wavenumber fictitious force method, the discrete wavenumber finite element method* and *the discrete wavenumber boundary element method.* This study uses the discrete wavenumber fictitious force method. Based on the moving Green's functions for a layered half-space and those for a cylinder of infinite length, boundary integral equations governing unknown fictitious forces (stresses) and tunnel-soil interaction stresses are established. Unlike the conventional boundary integral equation, those derived here only require the displacement Green's functions, not the stress Green's functions. This is achieved by introducing the excavated part of the ground as a separate substructure. The boundary integral equations are further transformed into a set of algebraic equations by expressing the displacement and stress along the tunnel-soil interface in terms of a Fourier series.

Results presented in this paper illustrate the effect of a tunnel on vibration propagation on the ground surface and the difference between a lined tunnel and an unlined tunnel. These results will be compared with those from the discrete wavennumber finite/boundary element model which is being developed.

CONTENTS

1. INTRODUCTION

An important issue with regard to the environmental impact of rail traffic is the problem of ground vibration produced by trains running in cut-and-cover or bored tunnels. The dominant frequencies associated with underground train-induced ground vibration are from about 15 Hz to 200 Hz [Grootenhuis, 1977]. Vibration in this range of frequency gives rise to structure borne or 'ground-borne' noise. To explore the mechanism of this problem, several models have been developed [Balendra *et al* 1989, 1991 and 1992; Jones *et al* 1999 and 2000; Forrest 1999; Metrikine *et al* 2000]. However, these models are either two-dimensional, therefore unable to account for the wave propagation in the third direction, or treat the ground as a whole-space, thus unable to model the wave reflection that is actually exists at the ground surface.

A model is required that can account not only for the wave propagation in the ground, but also for the movement of trains in the tunnel and wave propagation in the tunnel direction. The latter is important since the inclusion of a tunnel in the ground provides a waveguide in that direction. A three-dimensional model is therefore needed and for some studies is essential. A three-dimensional coupled finite/boundary element (FE/BE) model has recently been implemented for the case of stationary load [Andersen and Jones 2001] but is very expensive to use. In many situations, the geometry of the ground-tunnel structure can be considered to be invariant with respect to any translation along the tunnel axis. Utilisation of this feature may increase the computational efficiency, as suggested by for example Aubry [Aubry *et al* 1994]. In this idea, the problem is transformed into a sequence of two-dimensional models depending on wavenumbers in the tunnel direction. For each (discrete) wavenumber, the finite cross-section of the tunnel may be modelled using the FE method (called *the discrete wavenumber finite element method*, or *the two-dimensional finite element method*) and the wave propagation in the surrounding soil be modelled using the BE method (called *the discrete wavenumber boundary element method*, or *the two-dimensional boundary element method*). The simplicity of this approach comes from the fact that the discretization is only made over the cross-section of the ground/tunnel structure. The conventional two-dimensional finite and boundary element methods for the plane-strain problem, which corresponds to zero wavenumber, must be extended to account for any value of wavenumber. In addition to other issues, use of the discrete wavenumber boundary element method requires Green's functions, which are responses

(displacements and stresses) due to moving harmonic loads, either for a half-space or for a whole-space, expressed in terms of coordinates in the plane normal to the tunnel axis and the wavenumber in the tunnel direction. Such Green's functions for a layered half-space [Sheng, Jones and Petyt 1999] as well as for a homogeneous whole-space are now available [Sheng, Jones and Thompson 2002].

In addition to the discrete wavenumber finite/boundary element methods, an approach called *the discrete wavenumber fictitious force method* may also be used. This method was proposed by Luco *et al* [Luco and de Barros 1993] and is especially useful when the tunnel has a circular cross-section and the ground has a vertically layered structure. This method will be described and applied in this paper. It may provide a reference for the discrete wavenumber finite/boundary element methods. In the discrete wavenumber fictitious force method, a boundary integral equation governing unknown fictitious stresses and the tunnel-soil interaction stresses is established. The boundary integral equation developed by Luco *et al* [Luco and de Barros 1993], as that derived in the conventional boundary element method, not only requires the displacement Green's functions, but also requires the stress Green's functions. However in this paper, by regarding the excavated part (a solid cylinder of infinite length) of the ground as a separate substructure, the boundary integral equation only requires the displacement Green's functions of the ground (without the tunnel, therefore referred as to *the free ground*), the tunnel (a hollow circular cylinder, called *the tube* hereinafter) as well as the excavated cylinder. In the conventional boundary element method, the displacements and tractions on the boundary are interpolated using polynomials in terms of the values at nodes, and the boundary integral equation is then converted into a set of algebraic equations from which the values at the nodes can be determined. However in this paper, instead of using the interpolation method, the boundary integral equation is transformed into a set of algebraic equations by expressing every quantity in the boundary integral equation, which is a periodic function of positions on the tunnel-soil interface, in terms of a Fourier series. Each item of the Fourier series represents a harmonic component of that quantity and can be worked out from these algebraic equations.

In Section 2, analysis for each sub-structure is performed, and how the sub-structures are coupled to recover the actual situation is explained. The coupling procedure is detailed in Section 3, which leads to equations for the unknowns. Section 4 describes the calculation of the response of a horizontal plane in the ground (called *the observer*

plane, e.g. the ground surface). The case of a ground with an unlined tunnel is treated in Section 5. Results are presented in Section 6 to demonstrate the effect of the presence of a tunnel on the vibration propagation on the ground surface. Finally in Section 7, some conclusive marks are summarised.

2. ANALYSIS OF EACH SUB-STRUCTURE

A lined tunnel with a circular cross-section is called a tube hereinafter. The inner and outer radii of the tube are denoted by R_1 and R_2. The material properties of the tube are described by Young's modulus E_t, Possion ratio ν_t, density ρ_t and loss factor η_t.

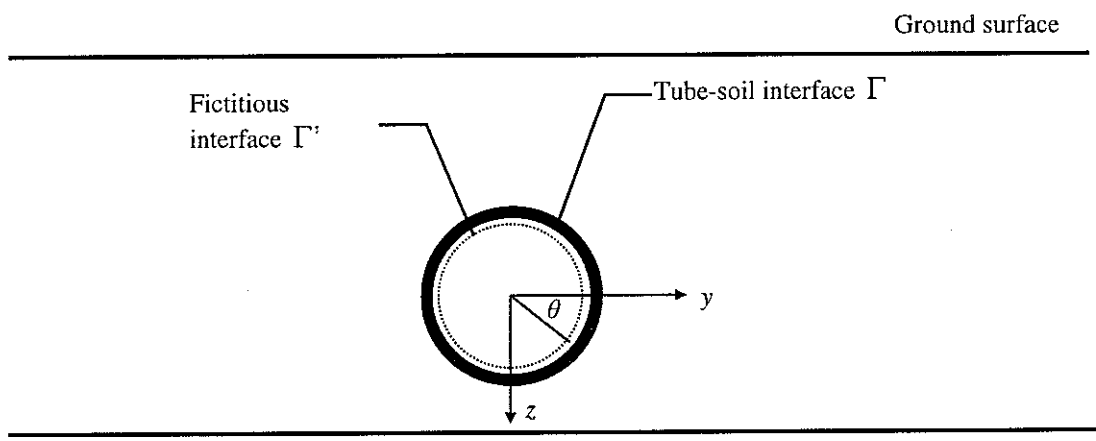

Figure 1. The ground/tunnel structure and the coordinate systems.

The ground is modelled as a vertically layered ground, consisting of a number, n, of layers. The nth layer overlies a homogeneous half-space or a rigid foundation, which is identified as the n+1th layer. The jth layer's material constants are: elastic modulus, E_j, Possion ratio, ν_j, density, ρ_j, loss factor, η_j, and thickness h_j. If the n+1th layer is a homogeneous half-space, its material constants are E_{n+1}, ν_{n+1}, ρ_{n+1} and η_{n+1}.

Three harmonic loads, $P_{x0}e^{i\Omega t}$, $P_{r0}e^{i\Omega t}$ and $P_{\theta 0}e^{i\Omega t}$, are applied at point ($R_1$, θ_0) on the inner surface of the tube. They are directed in the longitudinal (x-), radial and circumferential directions, respectively, as the notations indicate (Figure 1). The loads move over the inner surface of the tube in the x-direction at a constant speed c. The interface of the soil and the tube is denoted by Γ. The displacements of the tube-soil interface due to the moving loads are denoted by $w_x(x,\theta,t)$, $w_r(x,\theta,t)$ and $w_\theta(x,\theta,t)$ in accordance with the cylindrical coordinate system. The stresses on the tube-soil interface

due to the moving loads are denoted by $F_x(x,\theta,t)$ (i.e. τ_{xr}), $F_r(x,\theta,t)$ (i.e. σ_{rr}) and $F_\theta(x,\theta,t)$ (i.e. $\tau_{\theta r}$). The Fourier transforms of the displacements and the interaction stresses on the tube-soil interface are denoted by $\tilde{w}_x(\beta,\theta)$, $\tilde{w}_r(\beta,\theta)$, $\tilde{w}_\theta(\beta,\theta)$ and $\tilde{F}_x(\beta,\theta)$, $\tilde{F}_r(\beta,\theta)$, $\tilde{F}_\theta(\beta,\theta)$ (with the factor $\exp[i(\Omega-\beta c)]$ dropped, see [Sheng, Jones and Petyt 1999] and [Sheng, Jones and Thompson 2002]), where, β is the wavenumber in the x-direction.

2.1 ANALYSIS FOR THE TUBE

The Fourier transforms of the displacements of the tube are given by

$$\{\tilde{w}(\beta,\theta)\} = \sum_{m=-\infty}^{\infty}[\tilde{\Phi}(\beta,m)]e^{im(\theta-\theta_0)}\begin{Bmatrix}P_{x0}\\P_{r0}\\P_{\theta 0}\end{Bmatrix} + \int_0^{2\pi}\sum_{m=-\infty}^{\infty}[\tilde{\Phi}(\beta,m)]e^{im(\theta-\vartheta)}\begin{Bmatrix}\tilde{F}_x(\beta,\vartheta)\\\tilde{F}_r(\beta,\vartheta)\\\tilde{F}_\theta(\beta,\vartheta)\end{Bmatrix}R_2 d\vartheta \quad (1)$$

where, $[\tilde{\Phi}(\beta,m)]$ denotes the Fourier transformed moving dynamic flexibility matrix of the tube, of circumferential order m [Sheng, Jones and Thompson 2002], and

$$\{\tilde{w}(\beta,\theta)\} = (\tilde{w}_x(\beta,\theta),\tilde{w}_r(\beta,\theta),\tilde{w}_\theta(\beta,\theta))^T \quad (2)$$

In equation (1), the first term on the left side represents the response to the externally applied forces while the second one represents that due to the stresses on the tube-soil interface. Since $\tilde{F}_x(\beta,\theta)$, $\tilde{F}_r(\beta,\theta)$ and $\tilde{F}_\theta(\beta,\theta)$ are periodic functions of θ of period 2π, they may be expressed in terms of a Fourier series

$$\tilde{F}_x(\beta,\theta) = \sum_{k=-\infty}^{\infty}\tilde{F}_{xk}(\beta)e^{ik\theta} \quad (3)$$

$$\tilde{F}_r(\beta,\theta) = \sum_{k=-\infty}^{\infty}\tilde{F}_{rk}(\beta)e^{ik\theta} \quad (4)$$

$$\tilde{F}_\theta(\beta,\theta) = \sum_{k=-\infty}^{\infty}\tilde{F}_{\theta k}(\beta)e^{ik\theta} \quad (5)$$

Inserting equations (3) to (5) into equation (1), gives

$$\{\tilde{w}(\beta,\theta)\} = \sum_{m=-\infty}^{\infty}[\tilde{\Phi}(\beta,m)]e^{im(\theta-\theta_0)}\begin{Bmatrix}P_{x0}\\P_{r0}\\P_{\theta 0}\end{Bmatrix} + 2\pi R_2\sum_{m=-\infty}^{\infty}[\tilde{\Phi}(\beta,m)]e^{im\theta}\begin{Bmatrix}\tilde{F}_{xm}(\beta)\\\tilde{F}_{rm}(\beta)\\\tilde{F}_{\theta m}(\beta)\end{Bmatrix} \quad (6)$$

2.2 ANALYSIS FOR THE EXCAVATED CYLINDER

The ground with the infinitely long cylindrical hole of radius R_2 is subject to the action of the tube-soil interaction stresses $F_x(x,\theta,t)$, $F_r(x,\theta,t)$ and $F_\theta(x,\theta,t)$ on the wall of that cylindrical hole. For the ground without the hole (therefore it is called the *free ground*), a fictitious interface Γ' is defined and is located inside the tube-soil interface Γ (see Figure 1). The fictitious boundary Γ' and the tube-soil interface Γ are so close to each other that the radius of the former may be regarded as identical to that of the latter, i.e., R_2. On the fictitious interface Γ', fictitious moving forces (stresses), $T_x(x,\theta,t)$, $T_r(x,\theta,t)$ and $T_\theta(x,\theta,t)$, are applied. The Fourier transforms of the fictitious forces are denoted by $\tilde{T}_x(\beta,\theta)$, $\tilde{T}_r(\beta,\theta)$ and $\tilde{T}_\theta(\beta,\theta)$. Similar to equations (3), (4) and (5), they can be expressed as

$$\tilde{T}_x(\beta,\theta) = \sum_{k=-\infty}^{\infty}\tilde{T}_{xk}(\beta)e^{ik\theta} \quad (7)$$

$$\tilde{T}_r(\beta,\theta) = \sum_{k=-\infty}^{\infty}\tilde{T}_{rk}(\beta)e^{ik\theta} \quad (8)$$

$$\tilde{T}_\theta(\beta,\theta) = \sum_{k=-\infty}^{\infty}\tilde{T}_{\theta k}(\beta)e^{ik\theta} \quad (9)$$

If the fictitious forces are chosen in such a way that the stresses of the free ground on the tube-soil interface are the same as the actual tube-soil interaction stresses, i.e. $F_x(x,\theta,t)$, $F_r(x,\theta,t)$, $F_\theta(x,\theta,t)$, then the state (the displacement and stress fields) of the free ground outside Γ due to the fictitious forces is identical to that of the actual situation. When the fictitious interface Γ' approaches the tube-soil interface Γ, the fictitious forces on Γ' can be regarded as stresses externally applied on the outer surface of the excavated cylinder. Thus the total stresses on the outer surface of the excavated cylinder are $F_x(x,\theta,t)+T_x(x,\theta,t)$, $F_r(x,\theta,t)+T_r(x,\theta,t)$, $F_\theta(x,\theta,t)+T_\theta(x,\theta,t)$. The

Fourier transforms of the displacements of the outer surface of the excavated cylinder under the action of these stresses are given by

$$\{\tilde{w}(\beta,\theta)\} = \int_0^{2\pi} \sum_{m=-\infty}^{\infty} [\tilde{\Psi}(\beta,m)] e^{im(\theta-\vartheta)} \begin{Bmatrix} \tilde{F}_x(\beta,\vartheta)+\tilde{T}_x(\beta,\vartheta) \\ \tilde{F}_r(\beta,\vartheta)+\tilde{T}_r(\beta,\vartheta) \\ \tilde{F}_\theta(\beta,\vartheta)+\tilde{T}_\theta(\beta,\vartheta) \end{Bmatrix} R_2 d\vartheta \tag{10}$$

where, $[\tilde{\Psi}(\beta,m)]$ denotes the Fourier transformed moving dynamic flexibility matrix of the excavated cylinder, of circumferential order m. Having considered equations (3), (4), (5) and (7), (8), (9), equation (10) yields

$$\{\tilde{w}(\beta,\theta)\} = 2\pi R_2 \sum_{m=-\infty}^{\infty} [\tilde{\Psi}(\beta,m)] e^{im\theta} \begin{Bmatrix} \tilde{F}_{xm}(\beta)+\tilde{T}_{xm}(\beta) \\ \tilde{F}_{rm}(\beta)+\tilde{T}_{rm}(\beta) \\ \tilde{F}_{\theta m}(\beta)+\tilde{T}_{\theta m}(\beta) \end{Bmatrix} \tag{11}$$

2.3 ANALYSIS FOR THE FREE GROUND

The free ground is subject to the action of the fictitious forces. The Fourier transforms of the displacements of the free ground on the interface Γ due to the fictitious forces are given by

$$\{\tilde{w}(\beta,\theta)\} = \int_0^{2\pi} [\tilde{Q}_\Gamma(\beta,\theta,\vartheta)] \begin{Bmatrix} \tilde{T}_x(\beta,\vartheta) \\ \tilde{T}_r(\beta,\vartheta) \\ \tilde{T}_\theta(\beta,\vartheta) \end{Bmatrix} R_2 d\vartheta \tag{12}$$

where,

$$[\tilde{Q}_\Gamma(\beta,\theta,\vartheta)] = \begin{bmatrix} 1 & 0 & 0 \\ 0 & \cos\theta & \sin\theta \\ 0 & -\sin\theta & \cos\theta \end{bmatrix} \left(\frac{1}{2\pi} \int_{-\infty}^{\infty} [\tilde{Q}(\beta,\gamma,\theta,\vartheta)] e^{i\gamma R_2(\cos\theta-\cos\vartheta)} d\gamma \right) \begin{bmatrix} 1 & 0 & 0 \\ 0 & \cos\vartheta & -\sin\vartheta \\ 0 & \sin\vartheta & \cos\vartheta \end{bmatrix} \tag{13}$$

in which, $[\tilde{Q}(\beta,\gamma,\theta,\vartheta)]$ is the Fourier transformed moving dynamic flexibility matrix (or Green's functions) of the free ground, with the horizontal plane of observation at $z = R_2 \sin\theta$ and the loading position determined by $y = R_2 \cos\vartheta$ and $z = R_2 \cos\vartheta$. $[\tilde{Q}(\beta,\gamma,\theta,\vartheta)]$ is derived in reference [Sheng, Jones and Petyt 1999] in the Cartesian coordinate system and is a function of the wavenumbers β in the longitudinal direction

and γ in the lateral direction . The integral with respect to γ in equation (13) provides the Green's function transformed with respect to x only. Since the displacements and fictitious forces on the interface Γ are decomposed in accordance with the cylindrical coordinate system, a transformation between the Cartesian coordinate system and the cylindrical coordinate system must be introduced as indicated in equation (13). Following the properties explained in reference [Sheng, 2001] (Section 2.4.2 and equation (2.63)),

$$\begin{bmatrix} \tilde{Q}_{11} & \tilde{Q}_{12} & \tilde{Q}_{13} \\ \tilde{Q}_{21} & \tilde{Q}_{22} & \tilde{Q}_{23} \\ \tilde{Q}_{31} & \tilde{Q}_{32} & \tilde{Q}_{33} \end{bmatrix}_{(\beta,-\gamma,\theta,\vartheta)} = \begin{bmatrix} \tilde{Q}_{11} & -\tilde{Q}_{12} & \tilde{Q}_{13} \\ -\tilde{Q}_{21} & \tilde{Q}_{22} & -\tilde{Q}_{23} \\ \tilde{Q}_{31} & -\tilde{Q}_{32} & \tilde{Q}_{33} \end{bmatrix}_{(\beta,\gamma,\theta,\vartheta)} \tag{14}$$

$$\begin{bmatrix} \tilde{Q}_{11} & \tilde{Q}_{12} & \tilde{Q}_{13} \\ \tilde{Q}_{21} & \tilde{Q}_{22} & \tilde{Q}_{23} \\ \tilde{Q}_{31} & \tilde{Q}_{32} & \tilde{Q}_{33} \end{bmatrix}_{(\beta,\gamma,\vartheta,\theta)} = \begin{bmatrix} \tilde{Q}_{11} & \tilde{Q}_{21} & -\tilde{Q}_{31} \\ \tilde{Q}_{12} & \tilde{Q}_{22} & -\tilde{Q}_{32} \\ -\tilde{Q}_{13} & -\tilde{Q}_{23} & \tilde{Q}_{33} \end{bmatrix}_{(\beta,\gamma,\theta,\vartheta)} \tag{15}$$

Equation (14) shows that the Green's functions are even or odd with respect to γ while equation (15) represents a reciprocity relationship between the source and observer in the (β, γ) domain. It follows that

$$\begin{aligned} \int_{-\infty}^{\infty} [\tilde{Q}(\beta,\gamma,\theta,\vartheta)] e^{i\gamma R_2(\cos\theta-\cos\vartheta)} d\gamma = & \int_0^{\infty} \begin{bmatrix} \tilde{Q}_{11} & \tilde{Q}_{12} & \tilde{Q}_{13} \\ \tilde{Q}_{21} & \tilde{Q}_{22} & \tilde{Q}_{23} \\ \tilde{Q}_{31} & \tilde{Q}_{32} & \tilde{Q}_{33} \end{bmatrix}_{(\beta,\gamma,\theta,\vartheta)} e^{i\gamma R_2(\cos\theta-\cos\vartheta)} d\gamma \\ & + \int_0^{\infty} \begin{bmatrix} \tilde{Q}_{11} & -\tilde{Q}_{12} & \tilde{Q}_{13} \\ -\tilde{Q}_{21} & \tilde{Q}_{22} & -\tilde{Q}_{23} \\ \tilde{Q}_{31} & -\tilde{Q}_{32} & \tilde{Q}_{33} \end{bmatrix}_{(\beta,\gamma,\theta,\vartheta)} e^{-i\gamma R_2(\cos\theta-\cos\vartheta)} d\gamma \end{aligned} \tag{16}$$

$$\begin{aligned} \int_{-\infty}^{\infty} \begin{bmatrix} \tilde{Q}_{11} & \tilde{Q}_{12} & \tilde{Q}_{13} \\ \tilde{Q}_{21} & \tilde{Q}_{22} & \tilde{Q}_{23} \\ \tilde{Q}_{31} & \tilde{Q}_{32} & \tilde{Q}_{33} \end{bmatrix}_{(\beta,\gamma,\vartheta,\theta)} e^{i\gamma R_2(\cos\vartheta-\cos\theta)} d\gamma = & \\ \int_{-\infty}^{\infty} \begin{bmatrix} \tilde{Q}_{11} & -\tilde{Q}_{21} & -\tilde{Q}_{31} \\ -\tilde{Q}_{12} & \tilde{Q}_{22} & \tilde{Q}_{32} \\ -\tilde{Q}_{13} & \tilde{Q}_{23} & \tilde{Q}_{33} \end{bmatrix}_{(\beta,\gamma,\theta,\vartheta)} & e^{i\gamma R_2(\cos\theta-\cos\vartheta)} d\gamma \end{aligned} \tag{17}$$

Equation (16) indicates that the integration over the whole γ-axis can be done over the positive half γ-axis, while equation (17) shows that the reciprocity relationship between

the source and the observer is kept. Use may be made of equations (16) and (17) to increase the calculation efficiency.

Since $[\tilde{Q}_\Gamma(\beta,\theta,\vartheta)]$ is a periodic function of both θ and ϑ of period 2π, it may be written that

$$[\tilde{Q}_\Gamma(\beta,\theta,\vartheta)] = \sum_{m,k=-\infty}^{\infty}[\tilde{Q}_\Gamma(\beta,m,k)]e^{i(m\theta+k\vartheta)} \tag{18}$$

where,

$$[\tilde{Q}_\Gamma(\beta,m,k)] = \frac{1}{4\pi^2}\int_{-\pi-\pi}^{\pi\ \pi}[\tilde{Q}_\Gamma(\beta,\theta,\vartheta)]e^{-i(m\theta+k\vartheta)}d\theta d\vartheta \tag{19}$$

With the substitution of equations (7), (8), (9) and (18), equation (12) becomes

$$\{\tilde{w}(\beta,\theta)\} = 2\pi R_2\sum_{m-\infty}^{\infty}\sum_{k=-\infty}^{\infty}[\tilde{Q}_\Gamma(\beta,m,-k)]\begin{Bmatrix}\tilde{T}_{xk}(\beta)\\ \tilde{T}_{rk}(\beta)\\ \tilde{T}_{\theta k}(\beta)\end{Bmatrix}e^{im\theta} \tag{20}$$

Due to the lack of a closed form for the matrix $[\tilde{Q}_\Gamma(\beta,\theta,\vartheta)]$, it can only be calculated numerically at discrete points (nodes). Suppose $[\tilde{Q}_\Gamma(\beta,\theta,\vartheta)]$ is evaluated at nodes (θ_j, ϑ_l) $(j,l = 1,2,\cdots 2N)$, where

$$\theta_j = (j - \mathrm{N})\Delta\theta - 0.5\Delta\theta \quad , \quad \vartheta_l = (l-N)\Delta\theta - 0.5\Delta\theta \ , \ \Delta\theta = 2\pi/2N \tag{21}$$

and equation (18) is approximated by truncating the Fourier series to a finite number, $2N$, terms, i.e.

$$[\tilde{Q}_\Gamma(\beta,\theta,\vartheta)] = \sum_{m,k=-(N-1)}^{N}[\tilde{Q}_\Gamma(\beta,m,k)]e^{i(m\theta+k\vartheta)} \tag{22a}$$

then $[\tilde{Q}_\Gamma(\beta,m,k)]$ is given by

$$[\tilde{Q}_\Gamma(\beta,m,k)] = \frac{1}{(2N)^2}\sum_{j,l=1}^{2N}[\tilde{Q}_\Gamma(\beta,\theta_j,\vartheta_l)]e^{-i(m\theta_j+k\vartheta_l)} \tag{22b}$$

To evaluate $[\tilde{Q}_\Gamma(\beta,\theta_j,\vartheta_l)]$ for $j, l = 1, 2 \ldots 2N$, $2N \times 2N$ calculations of equation (13) are required. However, by making use of equation (17), the number of calculations of equation (13) reduces to $N(2N + 1)$. Equation (22b) indicates that the calculation of $[\tilde{Q}_\Gamma(\beta,m,k)]$ can be performed using the FFT algorithm.

The choice of N depends on the frequency of excitation and the radius of the tunnel. The higher the frequency or the larger the radius of the tunnel, the greater will be the number N.

3. DETERMINATION OF THE TUBE-SOIL INTERACTION STRESSES AND THE FICTITIOUS FORCES

The tube-soil interaction stresses and the fictitious forces are unknowns and may be determined by (1) requiring the displacements on the outer surface of the tube to be the same as for the outer surface of the excavated cylinder and in turn, (2) requiring the displacements on the outer surface of the excavated cylinder to be equal to those of the free ground at the fictitious interface. These two requirements set up two boundary integral equations the integral trajectory of which is along the tube-soil interface (a circle), with unknowns being the tube-soil interaction stresses and the fictitious forces. The first boundary integral equation is equivalent to the algebraic equation obtained by equating equation (6) to equation (11), i.e.

$$[\tilde{\Phi}(\beta,m)]e^{-im\theta_0}\{P\} + 2\pi R_2[\tilde{\Phi}(\beta,m)]\{\tilde{F}_m(\beta)\} = 2\pi R_2[\tilde{\Psi}(\beta,m)]\left(\{\tilde{F}_m(\beta)\} + \{\tilde{T}_m(\beta)\}\right) \quad (23)$$

where,

$$\{P\} = (P_{x0}, P_{r0}, P_{\theta 0})^T \quad (24)$$

$$\{\tilde{F}_m(\beta)\} = (\tilde{F}_{xm}(\beta), \tilde{F}_{rm}(\beta), \tilde{F}_{\theta m}(\beta))^T \quad (25)$$

$$\{\tilde{T}_m(\beta)\} = (\tilde{T}_{xm}(\beta), \tilde{T}_{rm}(\beta), \tilde{T}_{\theta m}(\beta))^T \quad (26)$$

The second boundary integral equation is equivalent to the algebraic equation obtained by equating equation (11) to equation (27), i.e.

$$[\tilde{\Psi}(\beta,m)]\left(\{\tilde{F}_m(\beta)\} + \{\tilde{T}_m(\beta)\}\right) = \sum_{k=-(N-1)}^{N}[\tilde{Q}_\Gamma(\beta,m,-k)]\{\tilde{T}_k(\beta)\} \quad (27)$$

From equations (23) and (27)

$$[\tilde{\Phi}(\beta,m)]e^{-im\theta_0}\{P\}+2\pi R_2[\tilde{\Phi}(\beta,m)]\{\tilde{F}_m(\beta)\}=2\pi R_2\sum_{k=-(N-1)}^{N}[\tilde{Q}_\Gamma(\beta,m,-k)]\{\tilde{T}_k(\beta)\}$$

which gives

$$\{\tilde{F}_m(\beta)\}=[\tilde{\Phi}(\beta,m)]^{-1}\sum_{k=-(N-1)}^{N}[\tilde{Q}_\Gamma(\beta,m,-k)]\{\tilde{T}_k(\beta)\}-\frac{1}{2\pi R_2}e^{-im\theta_0}\{P\} \tag{28}$$

Inserting equation (28) into equation (27), for $m = -(N-1),\ldots, N$, yields

$$\sum_{k=-(N-1)}^{N}\left([\tilde{\Phi}(\beta,m)]^{-1}-[\tilde{\Psi}(\beta,m)]^{-1}\right)[\tilde{Q}_\Gamma(\beta,m,-k)]\{\tilde{T}_k(\beta)\}+\{\tilde{T}_m(\beta)\}=\frac{1}{2\pi R_2}e^{-im\theta_0}\{P\} \tag{29}$$

From equations (29) and (28) the tube-soil interaction stresses and the fictitious forces can be worked out. Since the flexibility matrices of the substructures are of order 3×3, equation (29) is of order $6N\times6N$.

4. DISPLACEMENTS OF AN OBSERVER PLANE IN THE GROUND

As has been stated in Section 2.2, the response of the ground with the tube is identical to that of the perfect ground due to the fictitious forces. The Fourier transforms (with respect to both x and y) of the displacements of the top interface of the l_Rth layer in the free ground due to the fictitious forces on the fictitious interface are given by

$$\begin{Bmatrix}\tilde{u}_{l_R0}\\ \tilde{v}_{l_R0}\\ \tilde{w}_{l_R0}\end{Bmatrix}=\int_0^{2\pi}[\tilde{Q}(\beta,\gamma,\vartheta)]e^{-i\gamma R_2\cos\vartheta}[T]\begin{Bmatrix}\tilde{T}_x(\beta,\vartheta)\\ \tilde{T}_r(\beta,\vartheta)\\ \tilde{T}_\theta(\beta,\vartheta)\end{Bmatrix}R_2d\vartheta \tag{30}$$

where, $[\tilde{Q}(\beta,\gamma,\vartheta)]$ is the Fourier transformed moving dynamic flexibility matrix of the free ground, with the source position corresponding to ϑ, and $[T]$ is the coordinate transformation matrix, given by

$$[T]=\begin{bmatrix}1 & 0 & 0\\ 0 & \cos\vartheta & -\sin\vartheta\\ 0 & \sin\vartheta & \cos\vartheta\end{bmatrix} \tag{31}$$

Since $[\tilde{Q}(\beta,\gamma,\vartheta)][T]e^{-i\gamma R_2\cos\vartheta}$ is a periodic function of ϑ of period 2π, it may be written that

$$[\tilde{Q}(\beta,\gamma,\vartheta)][T]e^{-i\gamma R_2\cos\vartheta} = \sum_{m=-\infty}^{\infty}[\tilde{Q}(\beta,\gamma,m)]e^{im\vartheta} \tag{32}$$

Inserting equations (7), (8), (9) and (32) into equation (30), gives

$$\begin{Bmatrix}\tilde{u}_{l_R0}\\ \tilde{v}_{l_R0}\\ \tilde{w}_{l_R0}\end{Bmatrix} = 2\pi R_2\sum_{m=-\infty}^{\infty}[\tilde{Q}(\beta,\gamma,-m)]\{\tilde{T}_m(\beta)\} \tag{33}$$

5. THE CASE OF AN UNLINED TUNNEL

If the tunnel is unlined, then the displacements of the free ground on the interface Γ under the action of the externally exerted moving loads and the fictitious moving forces $T_x(x,\theta,t)$, $T_r(x,\theta,t)$ and $T_\theta(x,\theta,t)$, are identical to those of the outer surface of the excavated cylinder due to the fictitious forces. The displacements of the free ground on Γ, similar to equation (20), can be written as

$$\{\tilde{w}(\beta,\theta)\} = 2\pi R_2\sum_{m-\infty}^{\infty}\sum_{k=-\infty}^{\infty}[\tilde{Q}_\Gamma(\beta,m,-k)]\{\tilde{T}_k(\beta)\}e^{im\theta} + \sum_{m-\infty}^{\infty}\sum_{k=-\infty}^{\infty}[\tilde{Q}_\Gamma(\beta,m,-k)]e^{-ik\theta_0}\{P\}e^{im\theta} \tag{34}$$

The displacements of the excavated cylinder, similar to equation (11), can be written as

$$\{\tilde{w}(\beta,\theta)\} = 2\pi R_2\sum_{m=-\infty}^{\infty}[\tilde{\Psi}(\beta,m)]e^{im\theta}\{\tilde{T}_m(\beta)\} \tag{35}$$

From equations (34) and (35)

$$2\pi R_2[\tilde{\Psi}(\beta,m)]\{\tilde{T}_m(\beta)\} = 2\pi R_2\sum_{k=-(N-1)}^{N}[\tilde{Q}_\Gamma(\beta,m,-k)]\{\tilde{T}_k(\beta)\} + \sum_{k=-(N-1)}^{N}[\tilde{Q}_\Gamma(\beta,m,-k)]e^{-ik\theta_0}\{P\}$$

i.e.

$$-[\tilde{\Psi}(\beta,m)]^{-1}\sum_{k=-(N-1)}^{N}[\tilde{Q}_{\Gamma}(\beta,m,-k)]\{\tilde{T}_k(\beta)\}+\{\tilde{T}_m(\beta)\}$$
$$=\frac{1}{2\pi R_2}[\tilde{\Psi}(\beta,m)]^{-1}\sum_{k=-(N-1)}^{N}[\tilde{Q}_{\Gamma}(\beta,m,-k)]e^{-ik\theta_0}\{P\} \tag{36}$$

from which $\{\tilde{T}_m(\beta)\}$ can be determined.

The displacements of the observer plane, similar to equation (33), are given by

$$\begin{Bmatrix}\tilde{u}_{l_R 0}\\ \tilde{v}_{l_R 0}\\ \tilde{w}_{l_R 0}\end{Bmatrix}=2\pi R_2\sum_{m=-\infty}^{\infty}[\tilde{Q}(\beta,\gamma,-m)]\left(\{\tilde{T}_m(\beta)\}+\frac{1}{2\pi R_2}e^{-im\theta_0}\{P\}\right) \tag{37}$$

6. VALIDATION AND EXAMPLE RESULTS

In this section, validation of the method is performed and example results are calculated for a ground with a lined tunnel with a radius of 3.5 m and for the same ground with an unlined tunnel of the same radius. The material properties of the ground are listed in Table 1 and those for the lined tunnel (tube) in Table 2. These parameters are adopted from reference [Jones, Thompson and Petyt 1999]. The axis of the tunnel is at 16.5 m below the ground surface. A unit vertical harmonic load is applied at the invert of the tunnel and therefore is at 20 m below the ground surface.

6.1 VALIDATION

To validate the approach developed in this paper and the computer program that implements the calculation, displacements are calculated for the ground surface due to a unit vertical harmonic load of 40 Hz moving at 100 m/s along a horizontal line passing through ($x = 0$, $y = 0$ and $z = 20$ m) and parallel to the x-axis (the xy plane coincides with the ground surface and the z-axis is directed downward). The material properties of the ground are chosen as those listed in Table 1. The response of the ground may be evaluated using two models, i.e. *the free ground model* and *the ground/unlined tunnel model*. Both the models should give almost the same results if the radius of the unlined tunnel in the ground/unlined tunnel model is small (e.g. 0.1 m). Results from these two models are presented in Figures 2 and 3. Figure 2 shows the vertical displacements along the x-axis on the ground surface. The longitudinal displacements along the x-axis on the

ground surface are shown in Figure 3. A good agreement between these two models is achieved.

TABLE 1
Parameters for the ground

Young's modulus ($\times 10^6$ Nm^{-2})	Possion's ratio	Density (kg/m^3)	Loss factor	P-wave speed (m/s)	S-wave speed (m/s)
1770	0.4	1700	0.15	1500	610

TABLE 2
Parameters for the lined tunnel

Young's modulus ($\times 10^6$ Nm^{-2})	Possion's ratio	Density (kg/m^3)	Loss factor	Inner radius (m)	Outer radius (m)
37600	0.15	2400	0.05	3.4	3.6

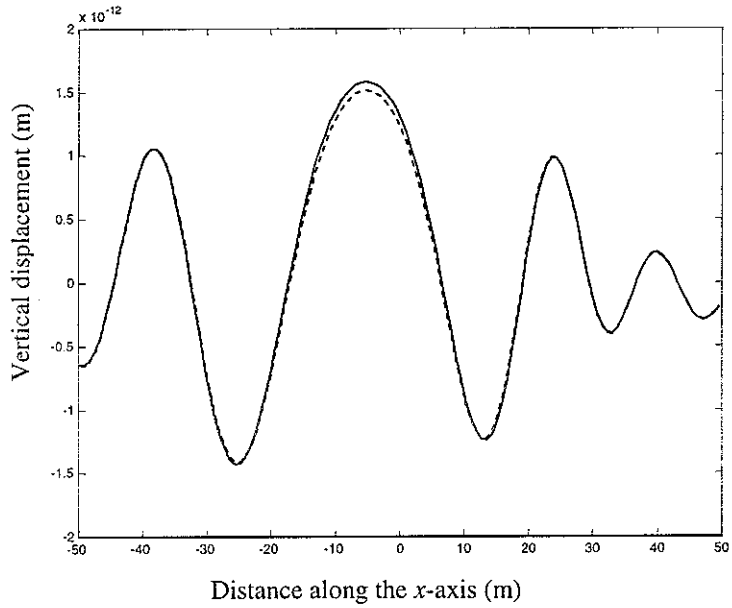

Figure 2. Vertical displacements along a straight line (y = 25 m) on the ground surface due to a unit vertical harmonic load of 40 Hz moving in the x-direction at 100 m/s at a depth of 20 m. ——, calculated using the free ground model; – – –, calculated using the *ground/unlined tunnel* model, with the radius of the tunnel being 0.1 m.

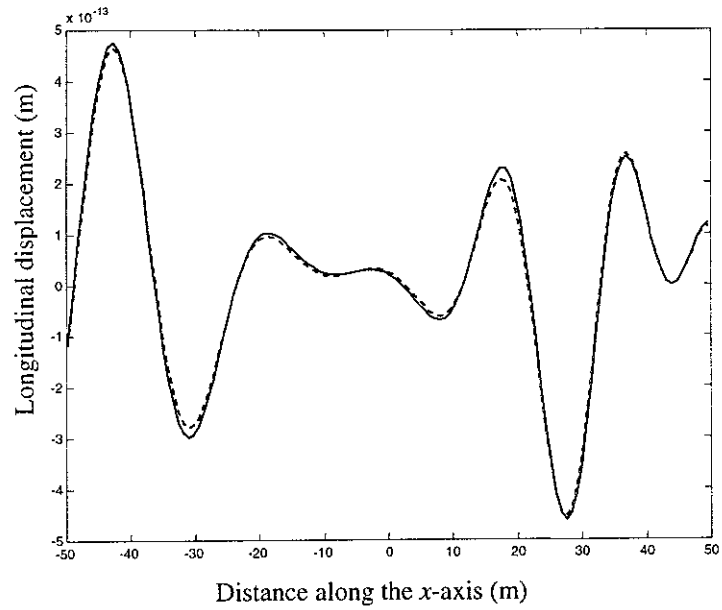

Figure 3. Longitudinal displacements along a straight line (y = 25 m) on the ground surface due to a unit vertical harmonic load of 40 Hz moving in the x-direction at 100 m/s at a depth of 20 m. ——, calculated using the free ground model; – – –, calculated using the *ground/unlined tunnel* model, with the radius of the tunnel being 0.1 m.

6.2 DISPERSION CURVES OF THE LINED TUNNEL (TUBE) AND GROUND

For the ground with the lined tunnel, both the dynamic properties of the tunnel (tube) and that of the ground (with a hole) affect the whole system. The dispersion curves of those two sub-structures may be used to interpret the results and therefore are presented in this sub-section.

6.2.1 *DISPERSION CURVES OF THE TUBE*

Figure 4 shows the dispersion curves of the tube. They are obtained by projecting the Fourier transformed radial displacements of the tube due to a radial harmonic load on the frequency-wavenumber plane. The displacements are calculated using the cylinder theory [Sheng, Jones and Thompson 2002] for different wavenumbers and different frequencies. Since the thickness of the tube (0.2 m) is small compared to its average radius (3.5 m), it may be regarded as a thin shell and the dispersion curves may be evaluated using one of the thin shell theories. Figure 5 presents the dispersion curves of the tube, of circumferential orders 0 to 8, calculated using the Donnel-Mushta thin shell theory [Leissa 1973]. Comparison between Figure 4 and Figure 5 shows that, the Donnel-Mushta theory gives highly precise results though it increases the cut-on (natural)

frequencies. The cut-on frequencies calculated using the Donnel-Mushta thin shell theory, are listed in Table 3.

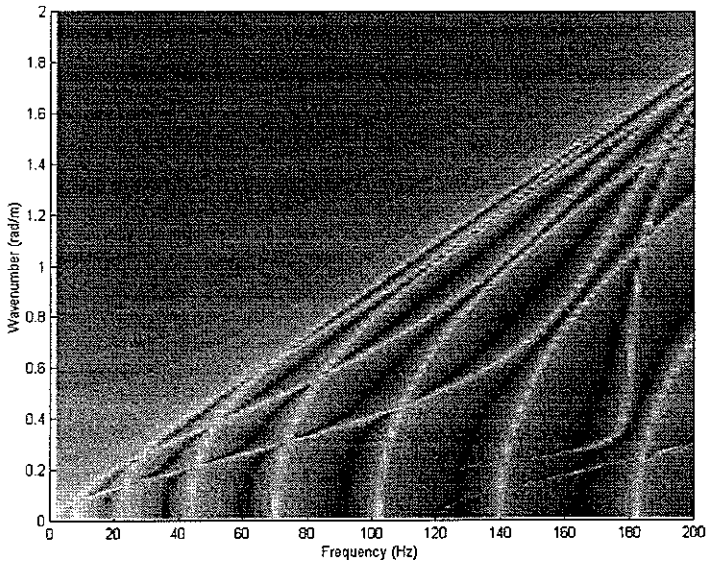

Figure 4. Dispersion curves of the tube (bright curves). They are obtained by projecting the Fourier transformed displacements, which are calculated using the cylinder theory for different wavenumbers and different frequencies, on the frequency-wavenumber plane.

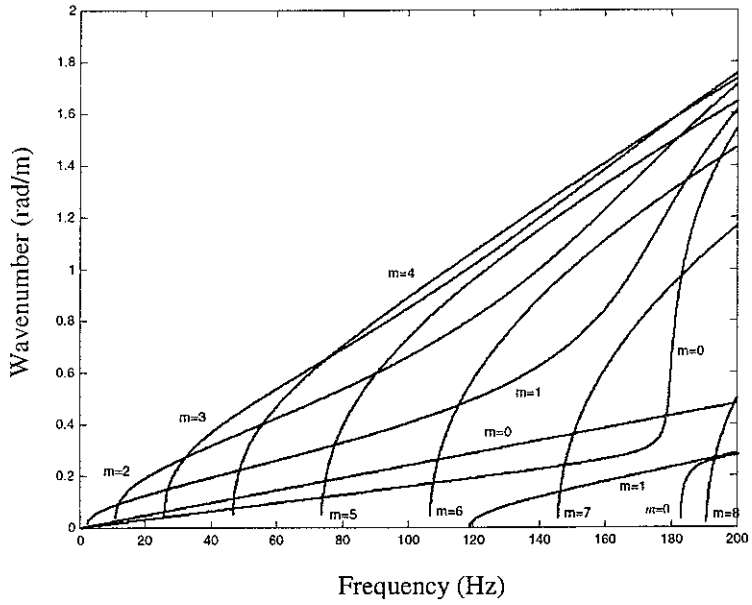

Figure 5. Dispersion curves of the tube of circumferential orders 0 to 8 , calculated using the Donnel-Mushta thin shell theory.

It can be seen from Table 3 that for circumferential order $m = 0 \sim 5$, the minimum cut-on frequencies of the ring modes range from 0 to 74 Hz, which is within the frequency range of interest for ground vibration induced by tunnel trains.

TABLE 3

Natural (cut-on) frequencies of the tube (from the Donnel-Mushta thin shell theory)

Circumferential order	Cut-on frequency (Hz) (Axial modes)	Cut-on frequency (Hz) (Radial modes)	Cut-on frequency (Hz) (Radial modes)
0	0	0	182.12
1	118.72	2.13	257.57
2	237.45	8.75	407.28
3	356.19	25.64	575.97
4	474.91	46.62	750.99
5	593.64	73.63	928.76

Two types of propagating waves are clearly shown in Figure 5 for circumferential order zero (i.e., the axially symmetric modes). For frequencies lower than 160 Hz, the two dispersion curves are straight lines. The upper straight line (first mode) represents the torsion waves while the lower straight line (second mode) represents the longitudinal waves. For a thin circular cylindrical shell, it can be shown that the dispersion equations for the longitudinal waves and the torsion waves are given by

$$\beta = 2\pi f \Big/ \sqrt{\frac{E}{(1-\nu^2)\rho}} \tag{38}$$

$$\beta = 2\pi f \Big/ \sqrt{\frac{E}{2(1+\nu)\rho}} \tag{39}$$

These two types of wave have small contributions to radial motions, especially for low frequencies as can be seen in Figure 4.

For circumferential order $m = 1$ (Figure 5), the waves of the first mode for low frequencies in the tube are close to the bending (flexural) waves of the tube when it is regarded as a beam. It should be noticed that, as shown by Gazis [Gazis 1959], the bending mode degenerates to a simple translation and hence zero frequency as the wavenumber decreases to zero whatever the thickness of the shell is. However, Figure 5 indicates a small cut-on frequency resulting from the 'thin shell theory'.

Figures 4 and 5 show that within 200 Hz, the propagating wavenumbers (β) are less than 2 rad/m. In other words, the wavelengths in the axial direction are greater than about 3.14 m.

6.2.2 *DISPERSION CURVES OF THE GROUND WITH A HOLE*

It is difficult to calculate the dispersion curves of a half-space with an unlined tunnel (a hole). Instead, the dispersion curves of a whole-space of the same material with the same hole are computed using the cylinder theory presented in reference [Sheng, Jones and Thompson 2002]. Figure 6 shows the results of such a calculation. The bright curve indicates the dispersion curve of the whole-space with an unlined tunnel of radius 3.5 m. Also shown in this figure are the Rayleigh wave dispersion curve of the material and the shear wave dispersion curve of the material. It can be seen that, the waves propagate along the hole in the whole-space at phase speeds which are between the Rayleigh wave speed and the shear wave speed. This kind of waves are called tube waves [Aki and Richards 1980] which propagate along the axis of the hole with energy confined to the vicinity of the hole. They exhibit dispersion with phase velocity increasing with wavelength. At wavelengths much shorter than the radius of the hole, they approach the Rayleigh wave of the material. The phase speed reaches the shear wave speed at a wavelength of about three times the radius (in the present case, this is about 10 m, or alternatively, the wavenumber is about 0.6 rad/m). Beyond this cut-off wavelength, they attenuate quickly by radiating S-waves.

Figures 4 and 6 indicate that, along the axis of the tube waves in the tube propagate faster than those in the ground.

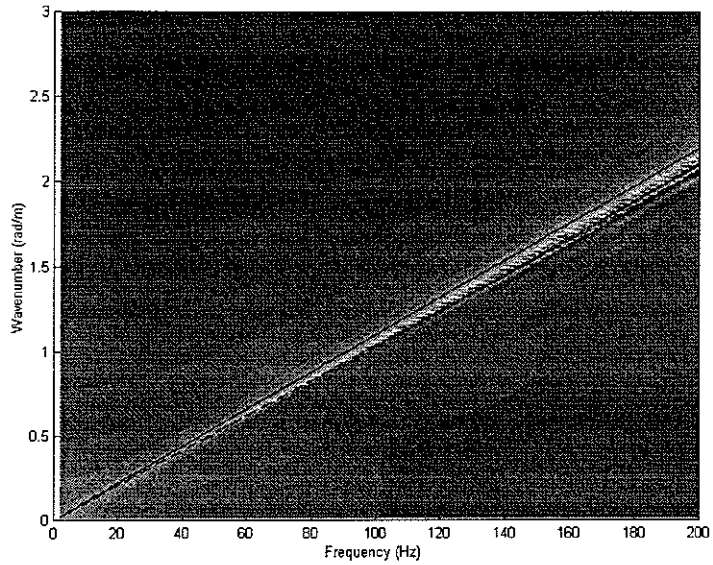

Figure 6. Dispersion curve (bright line) of the whole-space with an unlined tunnel of radius 3.5 m. It is obtained by projecting the Fourier transformed displacements of the hole surface, which are calculated using the cylinder theory for different wavenumbers and different frequencies, on the frequency-wavenumber plane. Also shown are the Rayleigh wave of the material (——) and the shear wave of the material (– – –).

6.3 RESPONSES TO A VERTICAL STATIONARY HARMONIC LOAD OF 200 HZ

Calculation has been carried out for a unit vertical stationary harmonic load of 200 Hz. The load is applied at the invert of the tunnel. Figure 7 shows the amplitudes of the vertical displacements on the ground surface for the lined tunnel. Those for the unlined tunnel are shown in Figure 8. It can be seen that, due to the presence of the tunnel, the propagation property in the tunnel direction and in the lateral direction (normal to the tunnel) is quite different. This is more obvious for the unlined tunnel. For waves to be clearly seen, Figures 9 and 10 show instantaneous vertical displacements along the x- and y-axes.

For the ground with the unlined tunnel, the wavelength at large distance in the lateral direction is about 3 m (Figure 10). This wave corresponds to the shear wave of the ground (the shear wave speed is 610 m/s, as indicated in Table 1, and the wavelength at 200 Hz is about 3 m). The wavelength in the x-direction has a longer wavelength 7.5 m (Figure 9), which corresponds to the P-wave in the ground. The tube wave propagating along the surface of the tunnel is confined to the vicinity of the hole and has insignificant contribution to the responses on the ground surface.

For the lined tunnel (tube), most modes have wavenumbers ranging from 1.4 rad/m to 1.8 rad/m (Figure 5), i.e. the wavelengths of the propagating waves in the tube ranges from 3.5 m to 4.5 m, shorter than the diameter (7 m) of the tube. This is the reason for the more nearly circular wave field on the ground surface for the lined tunnel than for the unlined tunnel (Figures 7 and 8).

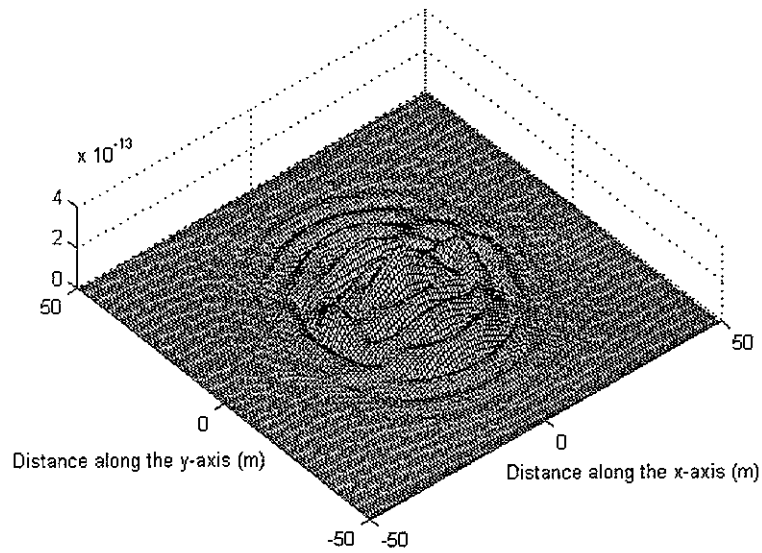

Figure 7. Vertical displacement amplitudes (in metres) on the ground surface due to a unit vertical harmonic stationary load of 200 Hz acting at the invert of the lined tunnel.

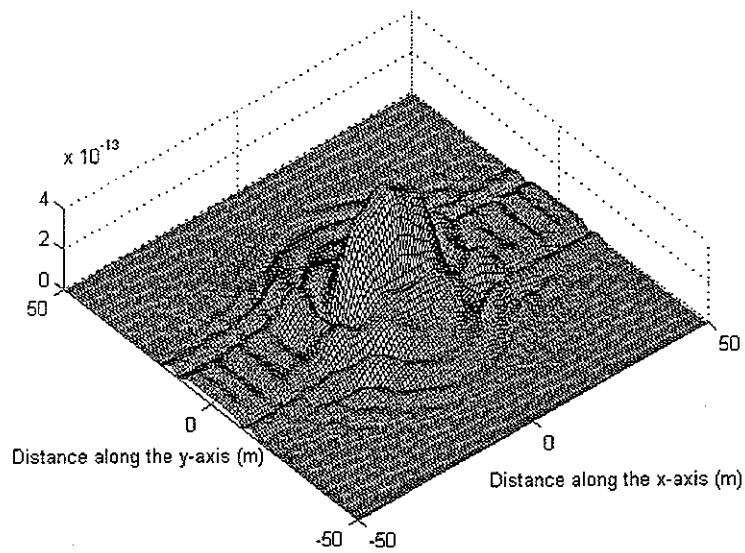

Figure 8. Vertical displacement amplitudes (in metres) on the ground surface due to a unit vertical harmonic stationary load of 200 Hz acting at the invert of the unlined tunnel.

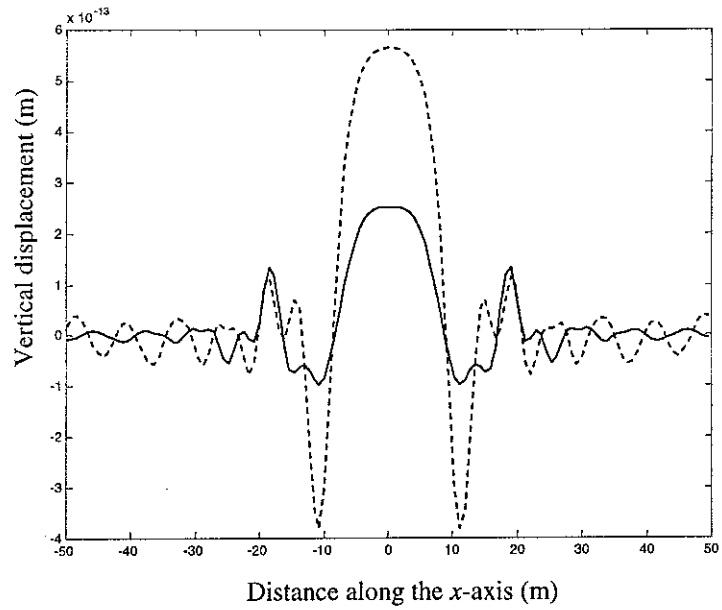

Figure 9. Vertical displacements along the x-axis on the ground surface due to a unit vertical harmonic stationary load of 200 Hz. ——, for the ground with the lined tunnel; – – –, for the ground with the unlined tunnel.

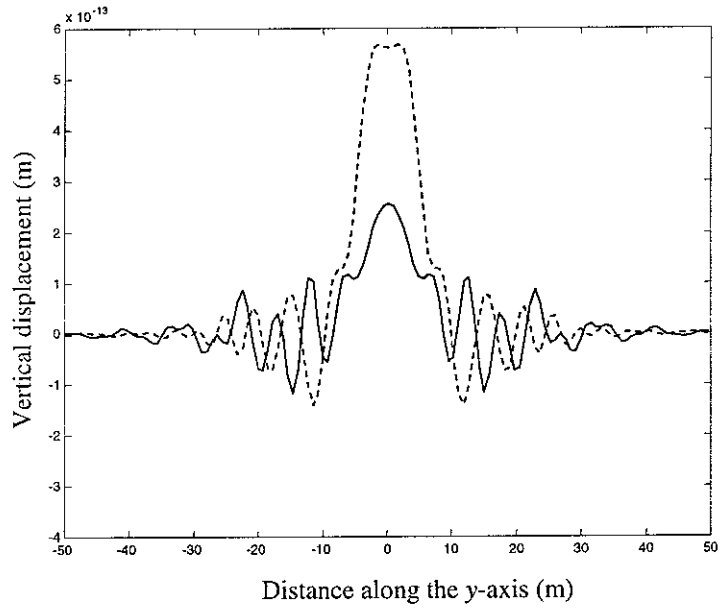

Figure 10. Vertical displacements along the y-axis on the ground surface due to a unit vertical harmonic stationary load of 200 Hz. ——, for the ground with the lined tunnel; – – –, for the ground with the unlined tunnel.

Figures 11 and 12 show the vertical displacement amplitudes along the x- and y-axes on the ground surface. It can be seen that beyond 20 m from the load, the responses along the x-axis for the lined tunnel are less than those for the unlined tunnel. The reverse is true for the responses along the y-axis.

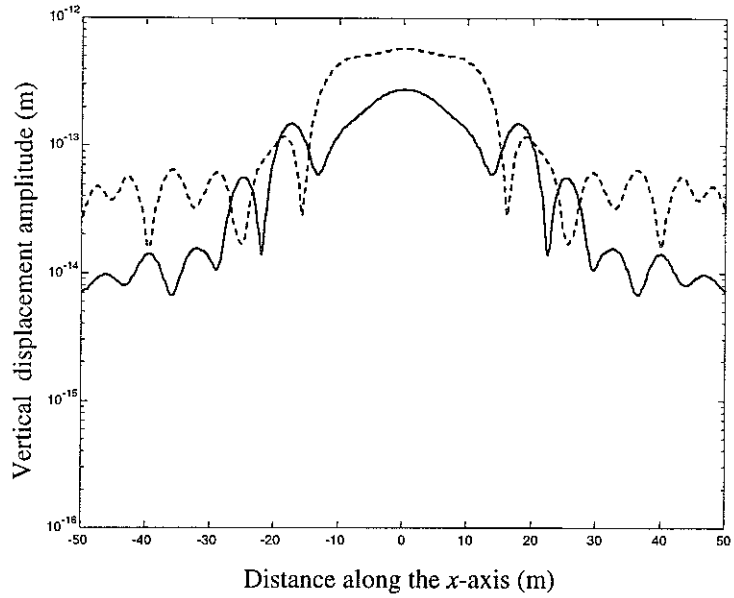

Figure 11. Vertical displacement amplitudes along the x-axis on the ground surface due to a unit vertical harmonic stationary load of 200 Hz. ——, for the ground with the lined tunnel; – – –, for the ground with the unlined tunnel.

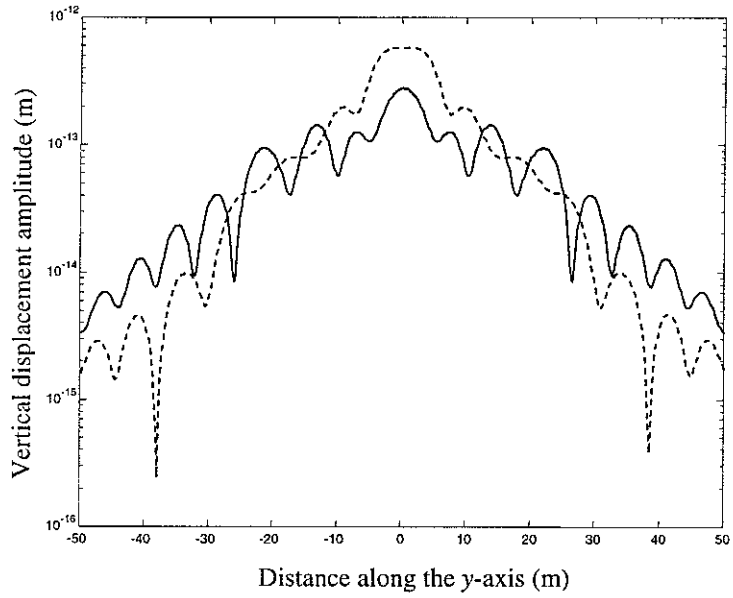

Figure 12. Vertical displacement amplitudes along the y-axis on the ground surface due to a unit vertical harmonic stationary load of 200 Hz. ——, for the ground with the lined tunnel; – – –, for the ground with the unlined tunnel.

6.4 RESPONSES TO A VERTICAL STATIONARY HARMONIC LOAD OF 40 HZ

Figures 13 and 14 show the amplitudes of the vertical displacements of the ground surface due to a unit vertical stationary harmonic load of 40 Hz exerted at the

tunnel invert. Figure 13 is for the lined tunnel while Figure 14 for the unlined tunnel. It can be seen that the lined tunnel greatly reduces the response at this frequency on the ground surface compared with the unlined tunnel, especially immediately above the tunnel. This is due to the bending stiffness of the lined tunnel (tube).

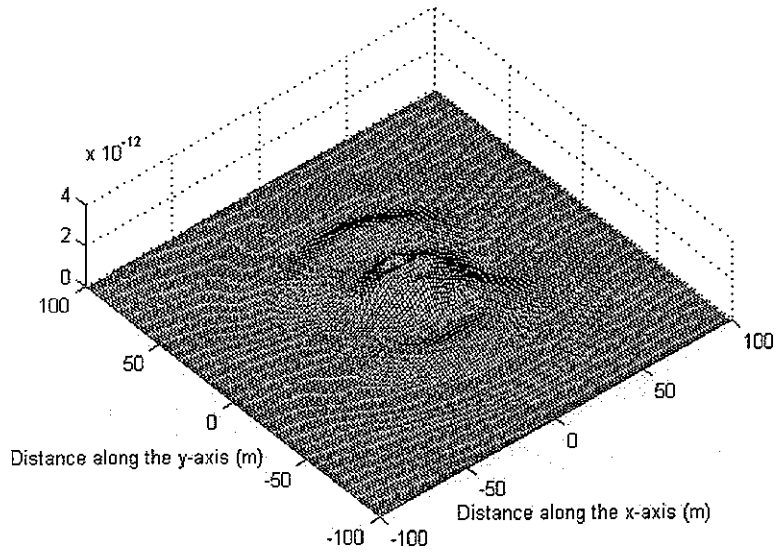

Figure 13. Vertical displacement amplitudes (in metres) of the ground surface due to a unit vertical stationary harmonic load of 40 Hz applied at the invert of the lined tunnel.

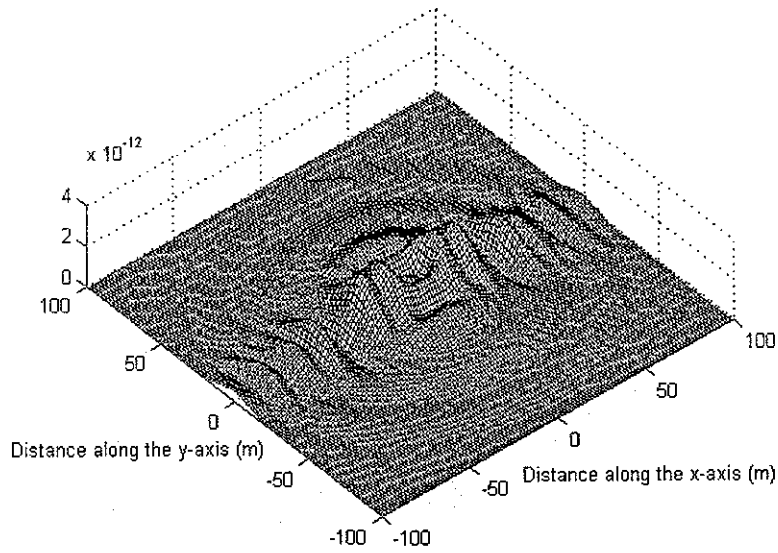

Figure 14. Vertical displacement amplitudes (in metres) of the ground surface due to a unit vertical stationary harmonic load of 40 Hz applied at the invert of the unlined tunnel.

6.5 RESPONSES TO A VERICAL MOVING HARMONIC LOAD OF 40 HZ

The amplitudes of the vertical displacement of the ground surface due to a unit vertical harmonic load of 40 Hz, which is exerted at the tunnel invert and moves in the tunnel direction at 100 m/s, are presented in Figures 15 and 16. Comparison between the lined tunnel and unlined tunnel for displacements along the x-and y-axes are shown in Figures 17 and 18.

These results reveal that the difference in the behaviour of the two tunnels is much greater in the direction along the tunnel axis than in the direction normal to it. Immediately above the load, at this frequency and load speed, the response levels from the lined and unlined tunnels are similar. However, Figure 17 shows a much stronger decay of vibration on the ground surface along the tunnel alignment for the lined tunnel than for the unlined one. This is due to the bending stiffness of the tube. Because of the speed of the load, a greater vibration level is observed behind the load than in front. Turning to the behaviour in the lateral direction, Figure 18 shows a similar overall decay of vibration on the ground surface for both of the tunnels.

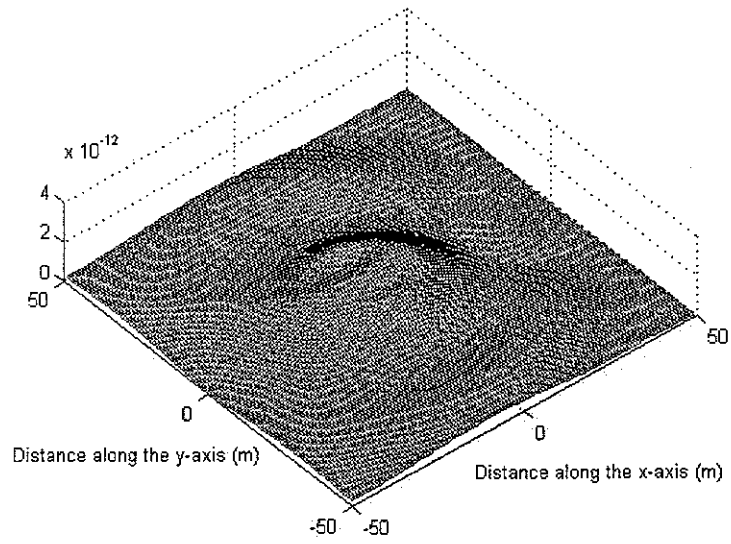

Figure 15. Vertical displacement amplitudes (in metres) of the ground surface due to a unit vertical harmonic load of 40 Hz. The load is applied at the invert of the lined tunnel and moves at 100 m/s in the tunnel direction.

Generally the results indicate that modelling the tunnel lining is important, especially for the behaviour of the field in the tunnel direction. This finding demonstrates the importance to model ground vibration from tunnel three-dimensionally.

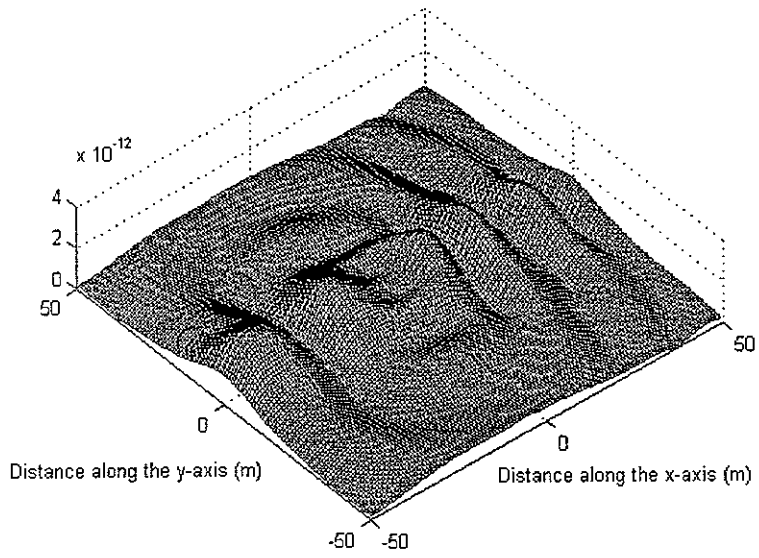

Figure 16. Vertical displacement amplitudes (in metres) of the ground surface due to a unit vertical harmonic load of 40 Hz. The load is applied at the invert of the unlined tunnel and moves at 100 m/s in the tunnel direction.

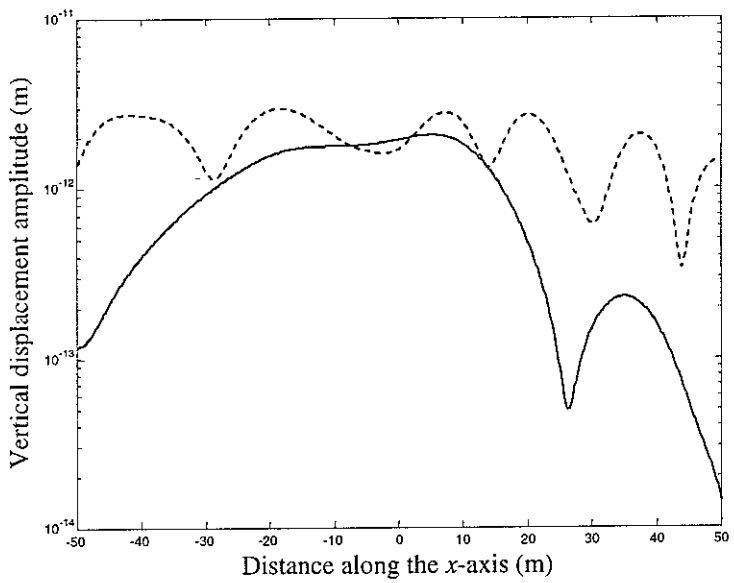

Figure 17. Vertical displacement amplitudes along the x-axis on the ground surface due to a unit vertical harmonic load of 40 Hz moving at 100 m/s at a depth of 20 m. ——, for the ground with the lined tunnel; – – –, for the ground with the unlined tunnel.

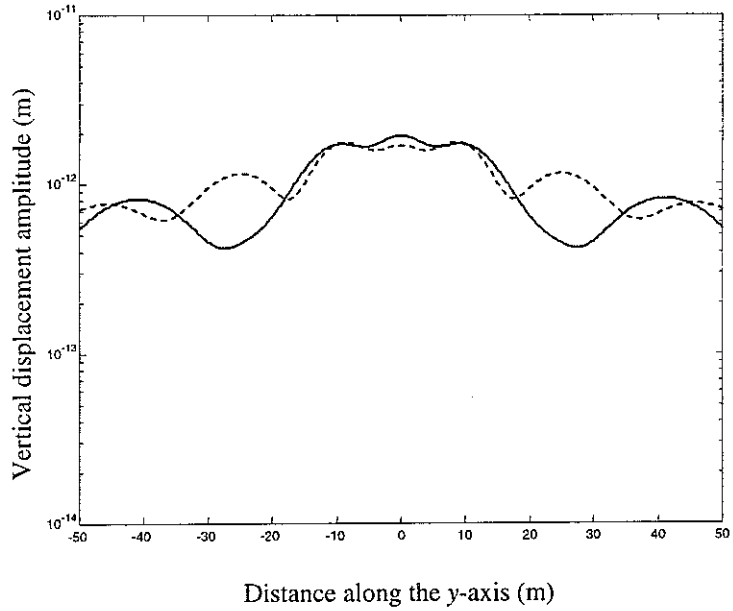

Figure 18. Vertical displacement amplitudes along the y-axis on the ground surface due to a unit vertical harmonic load of 40 Hz moving at 100 m/s at a depth of 20 m. ——, for the ground with the lined tunnel; – – –, for the ground with the unlined tunnel.

7. CONCLUSIONS

In this paper, the discrete wavenumber fictitious force method has been applied to develop a mathematical model for predicting ground vibration generated by a stationary or moving harmonic load applied in a circular lined or unlined tunnel. In this model, moving Green's functions for a layered half-space and those for a circular cylinder of infinite length are employed to establish a boundary integral equation governing unknown fictitious forces (stresses). This boundary integral equation only requires the displacement Green's functions rather than both displacement and traction Green's functions that are required by the conventional boundary element technique. This advantage is achieved by the introduction of the excavated cylinder into consideration. By expressing the Green's functions and other terms in terms of Fourier series, the boundary integral equation is transformed into a set of algebraic equations from which the unknowns can be determined.

Results are produced from this model for a lined tunnel and an unlined tunnel of the same radius, for a high frequency 200 Hz and a low frequency 40 Hz. The wave propagation on the ground surface is greatly affected by the presence of the tunnel, especially in the tunnel direction. The waveguide effect of the unlined tunnel on the

ground surface is much stronger than that of the lined tunnel. The lined tunnel may reduce responses of the ground surface immediately above the tunnel. This reduction is greater for low frequencies due to the dominant bending mode of the tunnel lining. However, away from the tunnel on the ground surface, the lined tunnel may increase the responses at high frequencies due to its radiation of energy into the surrounding ground.

ACKNOWLEDGMENT

This work is supported by the EPSRC under research grant GR/R67309/01.

REFERENCE

Aki, K. and Richards, P. G. 1980 *W. H. Freeman and Company, San Francisco*, Quantitative Seismology, Theory and Methods.

Andersen, L. and Jones, C. J. C. 2001. *ISVR Technical Memorandum No. 867, University of Southampton.* Three-dimensional elastodynamics analysis using multiple boundary element domains.

Aubry, D., Clouteau, D. and Bonnet, G. 1994 *Wave Propagation and Reduction of Vibrations*, Chouw and Schmid edition, Berg-Verlag, Bochum, 109-121. Modelling of wave propagation due to fixed or mobile dynamic sources.

Balendra, T., Chua, K.H., Lo, K.W. and Lee, S.L. 1989 *Journal of Engineering Mechanics, ASCE*, **115**(1), 145-162. Steady-state vibration of subway-soil-building system.

Balendra, T., Koh, C. G. and Ho, Y. C. 1991 *Earthquake Engineering and Structural Dynamics* **20**, 275-291. Dynamic response of buildings due to trains in underground tunnels.

Chua, K.H., Balendra, T. and Lo, K.W. 1992 *Earthquake Engineering and Structural Dynamics* **21**, 445-460. Groundborne vibrations due to trains in tunnels.

Dominguez, J. (1993). Boundary Elements in Dynamics. *Elsevier Applied Science.*

Eason, G., Fulton, J. and Sneddon, I. N. 1955/1956 *Phil. Trans. Roy. Soc. London* **248** (A955), 575-607. The generation of waves in an infinite elastic solid by variable body forces.

Flügge, W. and Kelkar, V. S. 1968 *International Journal of Solids Structures* **4**, 397-420. The problem of an elastic circular cylinder.

Forrest, J.A. 1999 *PhD Dissertation, Cambridge University.* Modelling of ground vibration from underground railways.

Gazis, D. C. 1959 *Journal of the Acoustical Society of America* **31**(5), 568-578. Three-dimensional investigation of the propagation of waves in hollow circular cylinders. Part I: Analytical foundation. Part II: Numerical results.

Grootenhuis, P. 1977 *Journal of Sound and Vibration* **51**(3), 443-448. Floating track slab isolation for railway.

Jones, C.J.C., Thompson, D.J. and Petyt, M. 1999 *ISVR Technical Memorandum No. 844, University of Southampton.* Ground-borne vibration and noise from trains: Elastodynamic analysis using the combined boundary element and finite element methods.

Jones, C.J.C., Thompson, D.J. and Petyt, M. 2000 *Proceedings of Seventh International Congress on Sound and Vibration*, Garmisch-Partenkirchen, Germany, 2703-2710. Studies using combined finite element and boundary element model for vibration propagation from railway tunnels.

Leissa, A. W., 1973 Vibration of Shells. National Aeronautics and Space Administration.

Luco, J. E. and de Barros, F. C. P. 1993 *Soil Dynamics and Earthquake Engineering* **12**, 565-580. On the three-dimensional seismic response of a class of cylindrical inclusions embedded in layered media.

Metrikine, A.V. and Vrouwenvelder, A.C.W.M. 2000 *Journal of Sound and Vibration* **234**(1), Surface ground vibration due to a moving train in a tunnel: Two-dimensional model.

Mirsky, I. 1965 *The Journal of the Acoustical Society of America* **37**(6), 1016-1026. Wave propagation in transversely isotropic circular cylinders. Part I: Theory. Part II: Numerical results.

Sheng, X., Jones, C. J. C. and Thompson, D. J. 2002 *University of Southampton, Institute of Sound and Vibration Research, Technical Memorandum* 885. Moving Green's functions for a layered circular cylinder of infinite length.

Sheng, X. 2001 *PhD Thesis, Southampton University*. Ground vibration generated from trains.

Sheng, X., Jones, C.J.C. and Petyt, M.1999 *University of Southampton, Institute of Sound and Vibration Research, Technical Memorandum* 837. The Fourier transformed stationary and moving flexibility matrices of a layered ground.

Tadeu, A.J.B. and Kausel, E. *2000 Journal of Engineering Mechanics* **126**(10), 1093-1097. Green's functions for two-and-a-half-dimensional elastodynamic problems.

APPENDIX COMPUTER PROGRAM

A computer program has been produced using Fortran 77 to implement the model presented in this paper. It is initiated by typing *Tunnel_TGV* at the DOS prompt.

A.1 INPUT DATA

A number of parameters are required to be input from the keyboard following the prompts from the program. The 'user-computer dialogues' are listed in Table A.1.

A.2 OUTPUT DATA FILES

The output data files created by the program are all formatted files. Data are written consecutively using WRITE (*id*,'(E15.6)') *u*, where, *id* is the identifier of the file into which the data in variable *u* is written. Therefore for each line (record) only one value presents.

Magnitudes and phase angles of the actual displacements of the observer plane are calculated for each of the values of $x = -(ngrid/4-1)\times\Delta x,\cdots,0,\Delta x,\cdots,(ngrid/4)\times\Delta x$, and $y = -(ngrid/4-1)\times\Delta y,\cdots,0,\Delta x,\cdots,(ngrid/4)\times\Delta y$, and stored consecutively, where, $\Delta x = 2\pi/(2\times ngrid\times\Delta\beta)$, $\Delta y = 2\pi/(2\times ngrid\times\Delta\gamma)$ and $2ngrid$ is the number of the samples in the inverse FFT. The magnitudes of the longitudinal, lateral and vertical displacements of the ground are stored in files *u10.dsp*, *v10.dsp* and *w10.dsp*, and the phase angles are in *u10.pha*, *v10.pha* and *w10.pha*.

TABLE A.1

User-computer dialogues

On the screen	Data type	Explanations
Input px0, pr0, pt0 and sita0	Real	Load amplitudes in *x*-, radial and circumferential directions and the angle coordinate of the loading point.
Input frequency, speed, dbeta/2pi, dgama/2pi	Real	Load frequency, load speed and wavenumber (in *x*- and *y*-directions) spacing (in cycle/m)
Is there a tube? 1=yes, 0=no	Integer	If the tunnel is lined, input 1; otherwise input 0
Young's modulus, loss factor, Possion ratio, density, inner & outer radii, axis-depth of the tube	Real	If the tunnel is lined, this line appears. Parameter for the tube (lining). Axis-depth means the vertical distance from the axis of the tunnel to the ground surface.
Radius and axis-depth of the unlined tunnel	Real	If the tunnel is unlined, this line appears.
Young's modulus, loss factor, Possion ratio, density of the excavated cylinder	Real	Parameter for the excavated cylinder.
Please input the number of layers of the ground (For a homogeneous half-space, the number is zero)	Integer	
Input the parameters of layer E Zita Nu Rho H	Real	For each layer, input the Yong's modulus, loss factor, density and thickness.
Foundation elastic or rigid? 1=elastic, 0=no	Integer	If the layers overly a homogeneous half-space then input 1; if the layers overly a rigid foundation, input 0.
Input the observer-layer No. and local depth	Real	Input the number of the layer which includes the observer plane, and the vertical distance from the observer plane to the top interface of the layer. **For a homogenous half-space, the observer-layer No. must be 1.**
Input ngrid (<=1024), npoint (<=256), m_max(<npoint-1)	Integer	Where 2×*ngrid* equals the number of discrete wavenumbers; 2×*npoint* equals the number of nodes on the tunnel-soil interface; *m_max* represents the maximum circumferential order involved in the calculation. Typically, *ngrid* = 512 or 1024, *npoint* = 32 or 64, *m_max* = 30. *ngrid* and *npoint* must be a power of 2.
Input path and directory for the outputs	A character string (≤ 50)	e.g. c:\my_project